Human Molecular Genetics, 2009, Vol. 18, No. 21 **4066–4080**
doi:10.1093/hmg/ddp355
Advance Access published on July 29, 2009

Molecular correlates of axonal and synaptic pathology in mouse models of Batten disease

Catherine Kielar[1,†], Thomas M. Wishart[2,†], Alice Palmer[2], Sybille Dihanich[1], Andrew M. Wong[1], Shannon L. Macauley[3,4], Chun-Hung Chan[5], Mark S. Sands[3,4], David A. Pearce[5], Jonathan D. Cooper[1,†] and Thomas H. Gillingwater[2,*,†]

[1]Department of Neuroscience, Centre for the Cellular Basis of Behaviour, Institute of Psychiatry, King's College London, London SE5 9NU, UK, [2]Centre for Integrative Physiology, University of Edinburgh Medical School, Edinburgh EH8 9XD, UK, [3]Department of Internal Medicine and [4]Department of Genetics, Washington University School of Medicine, St Louis, MO, USA and [5]Centre for Neural Development and Disease, University of Rochester School of Medicine and Dentistry, Rochester, New York 14642, USA

Received June 25, 2009; Revised and Accepted July 26, 2009

Neuronal ceroid lipofuscinoses (NCLs; Batten disease) are collectively the most frequent autosomal-recessive neurodegenerative disease of childhood, but the underlying cellular and molecular mechanisms remain unclear. Several lines of evidence have highlighted the important role that non-somatic compartments of neurons (axons and synapses) play in the instigation and progression of NCL pathogenesis. Here, we report a progressive breakdown of axons and synapses in the brains of two different mouse models of NCL: *Ppt1*$^{-/-}$ model of infantile NCL and *Cln6*^{nclf} model of variant late-infantile NCL. Synaptic pathology was evident in the thalamus and cortex of these mice, but occurred much earlier within the thalamus. Quantitative comparisons of expression levels for a subset of proteins previously implicated in regulation of axonal and synaptic vulnerability revealed changes in proteins involved with synaptic function/stability and cell-cycle regulation in both strains of NCL mice. Protein expression changes were present at pre/early-symptomatic stages, occurring in advance of morphologically detectable synaptic or axonal pathology and again displayed regional selectivity, occurring first within the thalamus and only later in the cortex. Although significant differences in individual protein expression profiles existed between the two NCL models studied, 2 of the 15 proteins examined (VDAC1 and Pttg1) displayed robust and significant changes at pre/early-symptomatic time-points in both models. Our study demonstrates that synapses and axons are important early pathological targets in the NCLs and has identified two proteins, VDAC1 and Pttg1, with the potential for use as *in vivo* biomarkers of pre/early-symptomatic axonal and synaptic vulnerability in the NCLs.

INTRODUCTION

Batten disease, or neuronal ceroid lipofuscinosis (NCL), is the most frequent autosomal-recessive neurodegenerative disease of childhood (1). At least ten different forms of NCL exist, each occurring due to mutations in a different gene, but characterized by the accumulation of autofluorescent storage material (2,3). The different forms of this lysosomal storage disorder are classified by the age of onset of the symptoms, with an increasing number of variant forms being identified (2,3). However, the pathophysiological mechanisms underlying these devastating disorders remain unclear.

Infantile NCL (INCL) is the most prevalent form of NCL in Finland with an incidence of 1 : 20 000 (4). INCL is caused by

*To whom correspondence should be addressed. Tel: +44 1316503724; Fax: +44 1316504193; Email: t.gillingwater@ed.ac.uk
†The authors wish it to be known that, in their opinion, these authors contributed equally to this study.

mutations in the *CLN1* gene encoding palmitoyl protein thioesterase 1 (PPT1) a soluble lysosomal enzyme (5), whose function is to remove long-chain fatty acids from modified cysteine residues (6). Patients with INCL undergo normal development until around 12 months, with subsequent neuronal degeneration in the CNS leading to retinal degeneration and blindness, cognitive and motor deficits, seizures and a flat electroencephalogram by 3 years (7,8). These children may remain in a vegetative state for several years and with no effective treatment available will invariably die (9).

Mutations in the *CLN6* gene, located on chromosome 15q23 (10,11), cause a variant late infantile form of NCL (vLINCL). The *CLN6* gene codes for a highly conserved protein which localizes to the endoplasmic reticulum (12,13). However, as for many NCL proteins, the function of the CLN6 gene product is currently unknown. As in INCL, affected children develop normally but subsequently develop epilepsy and neuronal degeneration that lead to loss of vision and progressive mental and motor deterioration resulting in the patient existing in a vegetative state for several years before dying in their early teens (3).

Data regarding the important role that distal, non-somatic neuronal compartments (axons and synapses) play in the instigation and progression of NCL pathology is gradually emerging. For example, several NCL proteins are expressed in the synaptic compartments of neurons (14,15). Furthermore, early signs of synaptic dysfunction and degeneration have been demonstrated in Ppt1 deficient neurons *in vitro* (16) and synaptic and axonal pathology occur early on in disease progression in the congenital form of NCL (17) and synaptic involvement in a mouse model of INCL was also recently demonstrated (18). However, the mechanisms underlying axonal and synaptic vulnerability in the NCLs remain poorly understood and no molecular biomarkers currently exist capable of providing a readout of the vulnerability status of axonal and synaptic compartments. A better understanding of the cellular and molecular characteristics of axonal and synaptic vulnerability will therefore be important for our understanding of disease pathogenesis and the effective development of therapeutic compounds.

We have now undertaken a correlated cellular/molecular investigation into synaptic and axonal vulnerability in mouse models of INCL (Ppt1 deficient mice) and vLINCL (Cln6 deficient mice). The individual proteins chosen for examination in our molecular experiments were based upon proteins previously identified in mice carrying a spontaneous genetic mutation that confers protection on axons and synapses (but not neuronal soma) in both the central and peripheral nervous systems: the Wallerian degeneration slow (Wld^s) mutant mouse (19–22). The remarkable Wld^s phenotype delays the degeneration of axons and synapses in response to a wide range of traumatic, toxic and disease-inducing stimuli (23–26) and can be transferred across species including rodents and *Drosophila* (27,28). Although the precise mechanism of action of Wld^s remains controversial, several *in vivo* and *in vitro* genomic and proteomic studies have identified downstream modifications in the expression of genes and proteins (focused around cell-cycle status, cell stress and mitochondrial stability) that are robust indicators of modified axonal and synaptic vulnerability (29–31). We chose to study examples of these indicator proteins in mouse models of Batten disease so as to undertake 'hypothesis-driven' research specifically focused on proteins known to be robustly altered when axons and synapses change their vulnerability status (29–31). This approach allowed us to obtain sensitive measurements of expression levels for these candidate proteins and was deemed preferable to a more 'discovery-driven' approach using whole genome or proteome screens where specific details regarding synaptic and/or axonal genes and proteins may be missed.

We show that synaptic and axonal pathology can be identified early on in the disease time-course in both Ppt1 deficient and Cln6 deficient mice, and that the severity of this pathology increases as the disease progresses. Thalamic regions were more severely affected at earlier time-points than cortical regions in both mouse models. Expression levels of protein markers of axonal and synaptic vulnerability were also significantly modified at pre/early- symptomatic stages of disease progression in both mouse models of NCL. Once again, pronounced differences were observed between the thalamus and cortex. These data provide insights into the molecular pathways underpinning axonal and synaptic vulnerability in the NCLs and also identify potential biomarkers of early neuronal vulnerability in NCL pathology.

RESULTS

Progressive synaptic and axonal pathology in *Ppt1* deficient mice is evident from early-symptomatic time-points

To investigate synaptic changes within the thalamocortical system of *Ppt1* deficient mice, we stained sections from 1 (pre/early-symptomatic), 3, 5 and 7 (late-symptomatic)-month-old control and $Ppt1^{-/-}$ mice for a range of pre-synaptic markers. We used antibodies against the synaptic vesicle protein synaptobrevin, the pre-synaptic membrane protein synaptophysin and the SNARE complex protein SNAP25. Immunohistochemical staining for these proteins revealed a complex series of changes over time in *Ppt1* deficient mice. SNAP25 immunoreactivity was observed at similar levels in the VPM/VPL and LGNd nuclei of the thalamus of *Ppt1* deficient mice and control mice at 1 month of age (Fig. 1A). However, levels of SNAP25 were markedly reduced in the thalamus of *Ppt1* deficient mice from 3 months of age onwards, suggesting that synaptic pathology was present at early-symptomatic time-points (Fig. 1A). SNAP25 immunoreactivity continued to decrease at 5 and 7 months of age in $Ppt1^{-/-}$ mice (Fig. 1A). While loss of SNAP25 immunoreactivity was most pronounced in the VPM/VPL and LGNd nuclei of the thalamus, decreased immunoreactivity was not confined to these regions, with other thalamic nuclei and brain regions (e.g. cortex; see following section) showing changes, especially at later-symptomatic ages. Similar data were obtained from the VPM/VPL and LGNd nuclei of the thalamus for synaptophysin (data not shown). The overall intensity of staining for synaptobrevin was not markedly changed in VPM/VPL and LGNd of *Ppt1* deficient mice but large globular aggregates of synaptobrevin were evident around surviving neurons in the LGNd and VPM/VPL as early as 3 months of age (data not shown).

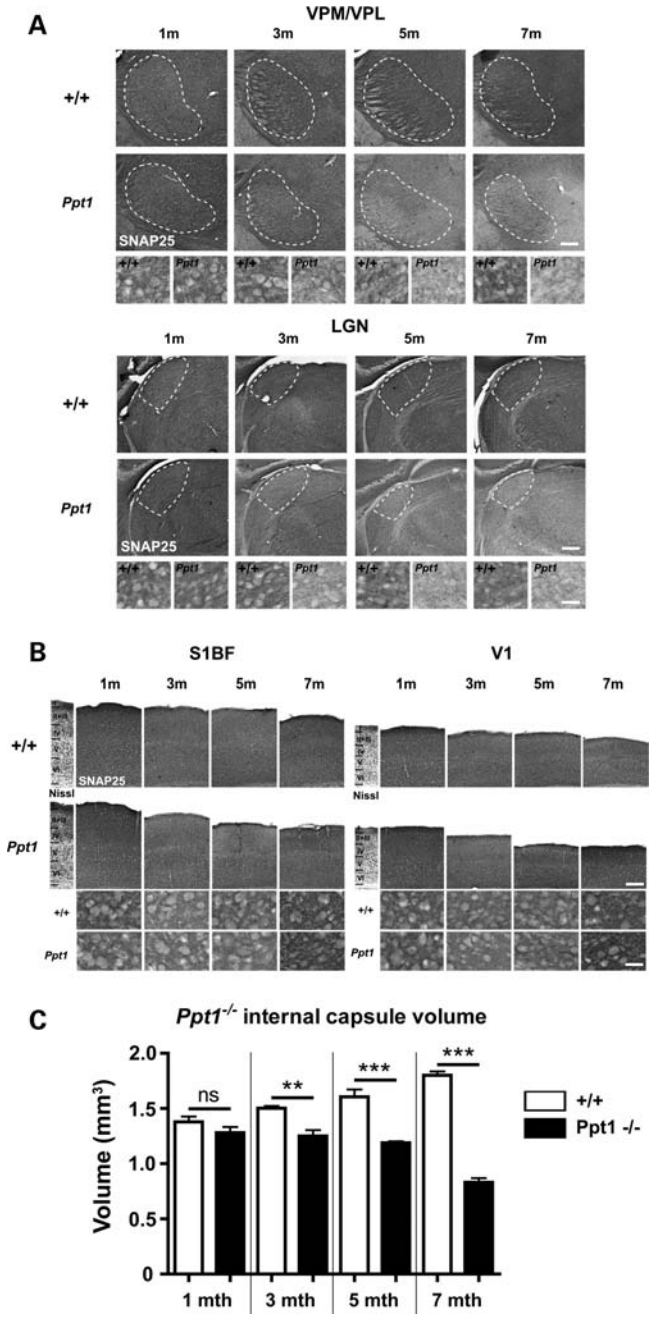

Figure 1. Effects upon SNAP25 expression in the visual and somatosensory system of *Ppt1* deficient mice. **(A)** Changes in the distribution and intensity of staining for SNAP25 in the ventral posteromedial and ventral posterolateral (VPM/VPL) and dorsal lateral geniculate (LGNd) thalamic nuclei of 1, 3, 5 and 7-month-old *Ppt1* deficient mice (*Ppt1*) and controls (+/+). Immunohistochemical staining for SNAP 25 within individual thalamic nuclei reveals similar levels of immunoreactivity in the VPM/VPL and LGNd of *Ppt1* deficient mice and control mice at 1 month of age. However, levels of SNAP25 were markedly reduced in the thalamus of *Ppt1* deficient mice from 3 months of age and continued to decrease with increased age in these mutant mice, as revealed in more detail at higher magnification. The boundaries of thalamic nuclei are indicated by white dashed lines. **(B)** SNAP25 immunoreactivity in the cortex was noticeably decreased by 3 months of age, but subsequently increased in intensity over time compared with age-matched control mice (+/+). Laminar boundaries are indicated by roman numerals on a Nissl-stained section through the same region of cortex. **(C)** Stereological survey of internal capsule volume in control and $Ppt1^{-/-}$ tissue at different stages of disease progression. The volume of the internal capsule was significantly reduced in $Ppt1^{-/-}$ mice versus controls from 3 months of age onwards. This reduction increased with time to reach a 40% difference between *Ppt1* deficient mice and age matched controls at 7 months of age. (mean $\pm$ SEM; $^{**}P < 0.01$; $^{***}P < 0.001$; ANOVA with *post-hoc* Bonferroni analysis). (**A** and **B**) show representative images from experiments on >3 mice per genotype. Scale bar = 200 μm in (**A** and **B**); 30 μm in higher magnification views.

The overall intensity of immunoreactivity for all three synaptic markers decreased in the cortex (motor and sensory areas) of $Ppt1^{-/-}$ mice, but not to the same extent as that observed in the thalamus (Fig. 1B). Both SNAP25 and synaptophysin immunoreactivity were noticeably decreased by 3 months of age in $Ppt1^{-/-}$ mice, but levels of both proteins subsequently increased over time (Fig. 1B and data not shown). Interestingly, we also noted an apparent reduction in SNAP25 expression in wild-type S1BF between 1 and 3 months (Fig. 1B), which may represent ongoing developmental remodelling of synapses in this region. In addition, increased synaptophysin staining was observed in lamina V compared with age-matched controls (data not shown). Synaptobrevin staining intensity was decreased from 3 months of age and decreased until 5 months, before subsequently increasing again at 7 months of age. As in the thalamus, large globular aggregates of synaptobrevin were evident in laminae IV and VI in both S1BF and V1 regions of cortex (data not shown).

To investigate if synaptic changes were accompanied by axonal degeneration, we carried out a stereological survey of internal capsule volume in Nissl-stained sections from control and *Ppt1* deficient mice at different stages of disease progression. The internal capsule was chosen for examination because it represents a large, easily identifiable white matter tract containing connections between the cortex and the thalamus. The volume of the internal capsule was significantly reduced in $Ppt1^{-/-}$ mice versus controls from 3 months of age onwards (Fig. 1C). This reduction in internal capsule volume increased with time to reach a 40% difference between *Ppt1* deficient mice and age-matched controls at 7 months of age (Fig. 1C).

Protein changes correlating with axonal and synaptic pathology in *Ppt1* deficient mice

We used quantitative immunofluorescent western blotting to directly determine relative protein expression levels between control and $Ppt1^{-/-}$ tissue at different stages of disease progression. A panel of 15 proteins was selected for investigation based upon their known responsiveness to changes in axonal and synaptic vulnerability (see Introduction; Table 1) (29–31). Seven of the proteins examined are involved in the regulation of cell cycle (H2Ax, H2B, BRCA2, cABL, Pttg1, Ccl3, acetyl H3), seven proteins are involved in synaptic function and stability (βSNAP, Sti1, GDI2, CRMP2P, VDAC1, VDAC2, CRMP2total) and one protein has been implicated in both cell-cycle regulation and synaptic form/function (Ube1) (29–31).

First, we examined protein expression levels in the thalamus of $Ppt1^{-/-}$ and control littermate mice (Table 2; Figs 2 and 3).

Table 1. Proteins selected for examination in the current study (all are known to have modified expression levels in mice expressing the Wld^S gene that protects axons and synapses from degeneration)

Protein	Direction of change (Wld^S)	Antibody source	Reference
Acetyl Histone H3	↑	Lake Placid Biologicals	31
Beta-SNAP	↑	Biomol International	30
BRCA2	↑	Abcam	31
cABL	↑	Abcam	31
Ccl3	↓	Abcam	31
CRMP2P	↑	Dr Calum Sutherland	30
CRMP2total	↑	Dr Calum Sutherland	30
GDI2	↓	Protein Tech Group	30
H2AX	↑	Upstate	31
Histone H2B	↑	Lake Placid Biologicals	31
Pttg1	↑	LabVision Corp.	29/31
Sti1	↓	BD Biosciences	30/31
Ube1	↑	Abcam	30/31
VDAC1	↓	GenTex	30
VDAC2	↑	Abcam	30

Although neither synaptic nor axonal pathology were readily identifiable in the thalamus of $Ppt1^{-/-}$ mice at 1 month of age, 66% of the proteins examined (10 out of 15) had expression levels modified by $>10\%$ in $Ppt1^{-/-}$ mice versus controls at 1 month of age (Fig. 3A; $\pm 10\%$ was selected as the minimum change required to be considered above background noise, based on low-level changes in control proteins such as tubulin). Five of these changes (33% of the 15 proteins examined) were found to be statistically significant (Table 2). The variability detected between samples in these experiments is likely to reflect the high sensitivity of some individual proteins (as is evident when observing dynamic temporal expression profiles in Fig. 3) to subtle differences in the rate of disease progression observed between animals.

Changes in protein expression were found in both cell-cycle-related and synaptic proteins (Fig. 3B and C). Expression levels for the majority of proteins were found to change dynamically with disease progression, with temporal expression profiles conforming to one of four 'templates'. Two proteins (H2AX and histone H2B) were found to have increasing expression levels over time (Fig. 3D). Five proteins (beta-SNAP, Sti1, GDI2, Ccl3 and acetyl histone H3) showed decreasing expression levels over time, albeit with Ccl3 and Sti1 starting from elevated expression levels at 1 month (Fig. 3E). The latter two proteins are both stress response proteins (32,33), so early expression changes may be reflecting a pre-symptomatic stress response. Four proteins (cABL, Ube1, Pttg1 and total CRMP-2) showed an 'up-down' expression profile (Fig. 3F). Interestingly, the peak in expression of these proteins at 3 months corresponded precisely with the onset of loss of synaptic markers in the thalamus (Fig. 1A). The remaining four proteins (VDAC1, VDAC2, BRCA2 and phosphorylated CRMP-2) showed relatively consistent changes in expression profiles throughout disease progression (Fig. 3G).

Next, we examined protein expression levels in the cortex of $Ppt1^{-/-}$ and control littermate mice (Table 3; Figs 4 and

Table 2. Protein expression levels in the thalamus of $Ppt1^{-/-}$ mice compared with wild-type littermates ascertained using quantitative fluorescent western blotting (*P*-values calculated using unpaired *t*-tests on raw arbitary fluorescence values from $Ppt1^{-/-}$ mice compared with wild-type littermate controls)

Protein	Age (months)	% change versus wild-type	S.E.	*P*-value
Acetyl Histone H3	1	−18.3	3.8	***
	3	−24.3	8.6	*
	5	−56.4	6.6	***
	7	−23	12.6	ns
Beta−SNAP	1	0.6	4.3	ns
	3	−13.8	1.2	***
	5	−24.6	3.4	***
	7	−20.9	3.1	***
BRCA2	1	31.5	20.6	ns
	3	11.3	10.6	ns
	5	14.9	3.9	**
	7	26.2	36.7	ns
cABL	1	18.4	16.2	ns
	3	32.9	32.9	ns
	5	8.9	7.6	ns
	7	−25.7	4.7	***
Ccl3	1	115.2	66.5	ns
	3	−21	1.9	***
	5	−2.7	16.6	ns
	7	106.3	50.9	ns
CRMP2P	1	−15.9	13.8	ns
	3	−1.6	5.2	ns
	5	−22	6.6	**
	7	−19.1	3	***
CRMP2total	1	−4.5	4.1	ns
	3	196.8	28.7	***
	5	−13.9	10.2	ns
	7	−21.6	5.1	***
GDI2	1	5.2	6	ns
	3	−15.1	6.5	*
	5	−12.5	2.9	***
	7	−25.5	20.9	***
H2AX	1	−3.6	9.3	ns
	3	7	7.6	ns
	5	8.5	7.4	ns
	7	18.8	20.9	ns
Histone H2B	1	−15.9	4.5	**
	3	13.2	14.8	ns
	5	18.5	25.7	ns
	7	81.6	60.5	ns
Pttg1	1	43.8	4.9	***
	3	87.3	33.8	*
	5	29.6	9.5	**
	7	−27.8	9.9	*
Sti1	1	66.5	8.7	***
	3	38.5	27.6	ns
	5	10.8	7.5	ns
	7	−27.1	6.4	***
Ube1	1	20.9	11.5	ns
	3	96.7	64.3	ns
	5	13.9	6.2	*
	7	−12.4	7.9	ns
VDAC1	1	42.9	8.6	***
	3	−1.3	18.8	ns
	5	34.2	7.7	***
	7	0.8	19.2	ns
VDAC2	1	7.6	6.9	ns
	3	−13.6	5.1	*
	5	−3.5	4.6	ns
	7	−13.9	5.8	*

$^*P < 0.05$; $^{**}P < 0.01$; $^{***}P < 0.001$.

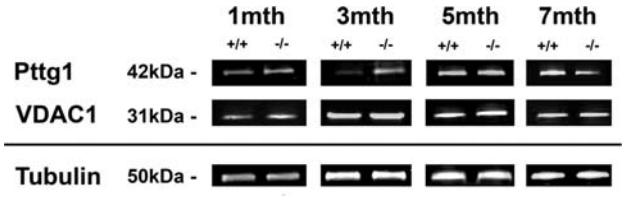

Figure 2. Representative fluorescent western blots of protein expression levels of Pttg1, VDAC1 and tubulin loading control in the thalamus of *Ppt1*$^{-/-}$ mice ($-/-$) and littermate controls ($+/+$) at 1, 3, 5 and 7 months.

5). As in the thalamus, 66% of the proteins examined (10 out of 15) had expression levels modified by $>10\%$ in *Ppt1*$^{-/-}$ mice versus controls at 1 month of age (Fig. 5A). Nine of these changes (60% of the 15 proteins examined) were found to be statistically significant (Table 3). Once again, changes in protein expression were observed in both cell-cycle-related and synaptic proteins (Fig. 5B and C). Expression levels for the majority of proteins were found to change dynamically with disease progression and the temporal expression profiles conformed to one of four templates. Examples of proteins conforming to the increasing, decreasing and no-change temporal profiles previously described in the thalamus were readily observed in the cortex (Fig. 5D, E and G). However, proteins conforming to an 'up-down' profile identified in the thalamus were not observed. In contrast, several of the proteins with 'up-down' expression profiles in the thalamus showed a mirror-image 'down-up' expression profile in the cortex (Ube1 and Pttg1; Fig. 5F).

Taken together, these experiments reveal robust early-onset protein expression changes correlating with synaptic and axonal pathology in the thalamus and cortex of *Ppt1*$^{-/-}$ mice *in vivo*. These data show that modified axonal and synaptic vulnerability in *Ppt1*$^{-/-}$ mice is accompanied by molecular changes in pathways including those regulating cell-cycle status and synaptic form/function.

Synaptic and axonal pathology in *Cln6* deficient mice mirrors events occurring in *Ppt1* deficient mice

In order to ask whether the axonal and synaptic changes observed within the thalamocortical system of *Ppt1* deficient mice were specific to INCL, or could be considered more ubiquitous pathological events occurring in other forms of NCL, we repeated our assessment of synaptic markers and internal capsule volume in *Cln6*^{nclf} mice modelling vLINCL.

Immunohistochemical staining for synaptic markers in 4 (pre/early-symptomatic) and 10 (late-symptomatic)-month-old *Cln6*^{nclf} mice revealed similar changes to those observed in *Ppt1* deficient mice. SNAP25 immunoreactivity was markedly reduced in the thalamus of *Cln6*^{nclf} mice at 4 months of age onwards, suggesting that synaptic pathology was present at early-symptomatic time-points (Fig. 6A). SNAP25 immunoreactivity continued to decrease at 10 months of age in *Cln6*^{nclf} mice (Fig. 6A). Similar data were obtained from the thalamus for synaptophysin (data not shown). The overall intensity of staining for synaptobrevin was not markedly changed in VPM/VPL and LGNd of *Cln6*^{nclf} mice, but large globular aggregates of synaptobrevin were evident around surviving neurons in the LGNd and VPM/VPL at 4 months of age already (data not shown).

In contrast to the thalamus, the overall intensity of immunoreactivity for all three synaptic markers increased in the cortex (both motor and sensory areas) of *Cln6*^{nclf} mice (Fig. 6B). Both SNAP25 and synaptophysin immunoreactivity were already elevated compared with controls at 4 months of age, and levels of both proteins subsequently increased further over time (Fig. 6B and data not shown). Increased synaptophysin staining was observed in laminae V and VI compared with age-matched controls (data not shown). Synaptobrevin staining intensity was slightly decreased at 4 months of age and subsequently increased at 10 months of age in laminae V and VI. As in the thalamus, large globular aggregates of synaptobrevin were evident in laminae V and VI in both S1BF and V1 regions of cortex (data not shown).

A stereological survey of axonal integrity (internal capsule volume) in Nissl-stained sections in control and *Cln6*^{nclf} mice at different stages of disease progression revealed a significant decrease in internal capsule volume with increasing disease progression in *nclf* mice compared with age-matched controls (Fig. 6C). A similar magnitude of reduction in internal capsule volume was noted for late-symptomatic *Cln6*^{nclf} mice ($\sim$30% difference; Fig. 6C) as was evident in *Ppt1* deficient mice (Fig. 1C).

Protein changes correlating with initiation of axonal and synaptic pathology in *Cln6* deficient mice

We next asked whether any of the early protein markers of axonal and synaptic vulnerability observed in the thalamus of pre/early-symptomatic (1 month old) *Ppt1* deficient mice were also modified in pre/early-symptomatic (3 month old) *Cln6*^{nclf} mice. This analysis was designed to reveal any significant convergence or divergence in the molecular pathways underpinning early changes in synaptic and axonal vulnerability in the NCLs. Any proteins identified as having similar modifications in expression profiles across both models of NCL would therefore have a strong case for being considered as potential 'biomarkers' of pre-symptomatic modifications in axonal and synaptic vulnerability *in vivo*.

We compared changes in expression levels within the thalamus for all 15 candidate proteins in 1 month old *Ppt1*$^{-/-}$ mice versus 3-month-old *Cln6*^{nclf} mice (Fig. 7). As with *Ppt1*$^{-/-}$ mice, the majority (14 out of 15) of proteins examined showed modifications in expression levels, with a magnitude $>10\%$ (Fig. 7A). All 14 changes were statistically significant (Fig. 7A). Two proteins showed consistent directional expression changes across both mouse models at these early-symptomatic time-points (Fig. 7B): voltage-dependent anion channel 1 (VDAC1) and pituitary tumor transforming gene 1 (Pttg1). However, the vast majority of proteins examined did not show similar expression profiles when comparing *Ppt1* deficient mice and *Cln6*^{nclf} mice (e.g. Ccl3 and Ube1; Fig. 7B). These data suggest that VDAC1 and Pttg1 might be useful as early biomarkers of modified axonal and synaptic vulnerability in the NCLs. They also imply that the molecular pathways regulating synaptic and axonal degeneration in INCL and vLINCL impact on similar cellular pathways

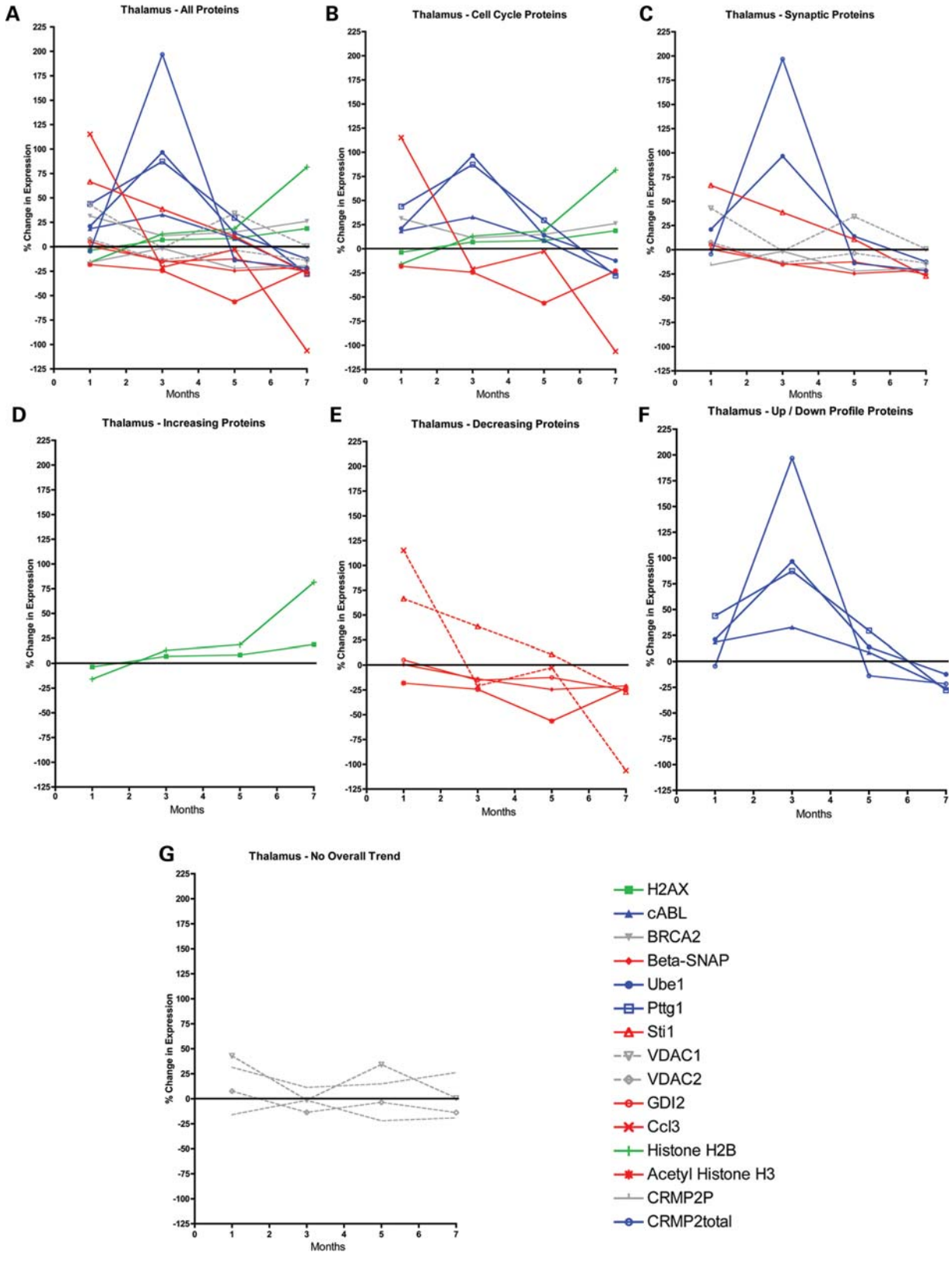

Figure 3. Temporal progression of protein expression changes in the thalamus of *Ppt1*$^{-/-}$ mice. (**A**) Temporal progression of expression profiles for all 15 proteins examined. This graph is included to illustrate the overall complexity of expression changes observed. Data for individual proteins is shown more clearly on the subsequent graphs. (**B**) Graph of cell cycle proteins only [data extracted from (A)]. (**C**) Graph of synaptic proteins only [data extracted from (A)]. (**D**–**G**) Graphs showing expression levels for proteins conforming to a 'increasing' profile (D), 'decreasing' profile (E), 'up-down' profile (F) or 'no overall trend' profile (G). Profiles were determined by the patterns of change in expression following initial measurements in 1-month-old mice, not by the initial direction of change. Note how proteins conforming to the 'up-down' profile reach their peak in 3-month-old mice. All data normalized to control tubulin levels.

Table 3. Protein expression levels in the cortex of $Ppt1^{-/-}$ mice compared with wild-type littermates ascertained using quantitative fluorescent western blotting (*P*-values calculated using unpaired *t*-tests on raw arbitary fluorescence values from $Ppt1^{-/-}$ mice compared with wild-type littermate controls)

Protein	Age (months)	% change versus wild-type	S.E.	*P*-value
Acetyl Histone H3	1	−18.1	12.2	ns
	3	−17.6	4.9	**
	5	0.8	8.9	ns
	7	13.9	17.9	ns
Beta-SNAP	1	2	6.5	ns
	3	−37.3	0.3	***
	5	−14.7	3.4	***
	7	−18.7	3.5	***
BRCA2	1	57.2	15.2	**
	3	−17.6	11	ns
	5	10.5	10.6	ns
	7	66.4	6.2	***
cABL	1	7.7	2.7	ns
	3	19.5	13.7	***
	5	20.1	9	ns
	7	12.8	18.6	ns
Ccl3	1	115.6	42.5	*
	3	−4.8	7.8	ns
	5	−0.2	5.4	ns
	7	−4.9	9.5	ns
CRMP2P	1	−8.9	3.7	*
	3	−26.4	2.4	***
	5	9.8	4.2	*
	7	−18.6	5.2	**
CRMP2total	1	−7	9	ns
	3	−14.7	7.4	ns
	5	12	11.4	ns
	7	−12.7	11.3	ns
GDI2	1	−29.7	7.3	***
	3	−40.4	2.1	***
	5	−28.5	6.7	***
	7	−8.7	5.1	ns
H2AX	1	12	10.5	*
	3	−22.3	6.8	**
	5	24.8	24.1	ns
	7	61.3	32.3	**
Histone H2B	1	−25.5	4	***
	3	−28.7	3.6	***
	5	−22.8	6.7	**
	7	−12	12.1	ns
Pttg1	1	56.2	14.6	**
	3	28.1	8.9	*
	5	23.8	20.8	ns
	7	79.9	34.2	*
Sti1	1	63.3	17.1	**
	3	19.3	12	ns
	5	144.3	40.6	**
	7	122.7	35.4	**
Ube1	1	43.7	15.5	*
	3	−58	4.4	***
	5	−8.7	7.9	ns
	7	67	21.4	**
VDAC1	1	4.7	18.2	ns
	3	−11.3	12.2	ns
	5	26.6	30.1	ns
	7	96.4	38.7	*
VDAC2	1	11.7	9.1	ns
	3	−12.7	3.3	**
	5	−4.5	2.4	ns
	7	−24	4.9	***

*$P < 0.05$; **$P < 0.01$; ***$P < 0.001$.

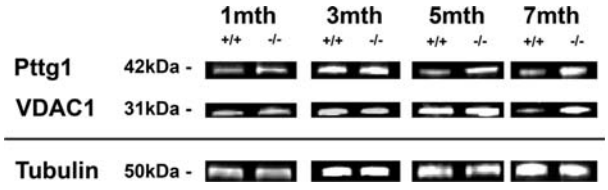

Figure 4. Representative fluorescent western blots of protein expression levels of Pttg1, VDAC1 and tubulin loading control in the cortex of $Ppt1^{-/-}$ mice (−/−) and littermate controls (+/+) at 1, 3, 5 and 7 months.

(e.g. cell cycle and synaptic stability), but with divergent responses in the levels of other individual proteins.

Finally, in order to confirm that VDAC1 and Pttg1 may be useful as clinically relevant biomarkers reporting on neuronal vulnerability status *in vivo*, we assessed protein expression levels in peripherally accessible tissue (muscle) from pre/early-symptomatic (1 month old) $Ppt1^{-/-}$ and wild-type littermate control mice ($n = 4$ mice per genotype; Fig. 8A). Both VDAC1 and Pttg1 showed significantly modified expression levels in hind-limb muscle preparations (including quadriceps, hamstrings, gastrocnemius and soleus) from $Ppt1^{-/-}$ mice compared with wild-type littermate controls (Fig. 8B and C). Interestingly, both proteins showed a similar magnitude of expression change to those observed in the thalamus. However, the direction of expression change in pathologically unaffected muscle tissue (T Gillingwater and J Cooper, unpublished observations) occurred in the opposite direction to those observed in the thalamus for both proteins. This may directly reflect the differing pathological status of the two tissues examined. Nevertheless, these data show that both VDAC1 and Pttg1 levels can be robustly determined in muscle and suggest that altered expression of these proteins in muscle may be useful as a biomarker for accompanying underlying changes in neuronal vulnerability.

DISCUSSION

The current study has generated three major conclusions. First, we have demonstrated that axonal and synaptic compartments of neurons are early pathological targets in two different mouse models of NCL, with the thalamus being particularly vulnerable at early stages of disease progression. Second, we have shown that a range of cell cycle and synaptic proteins known to be robust markers of axonal and synaptic vulnerability have regionally specific modified expression levels in NCL. Third, we have shown that two proteins (namely VDAC1 and Pttg1) have the potential to be used as biomarkers of pre/early-symptomatic changes in axonal and synaptic vulnerability in INCL and vLINCL *in vivo*.

In both mouse models of NCL examined, the onset of synaptic and axonal pathology was detectable at pre/early-symptomatic time-points. For example, we have demonstrated a reduced expression of key synaptic proteins (e.g. SNAP25) in the thalamus at pre/early-symptomatic ages as well as a reduction in the size of the internal capsule over time corresponding with disease progression. These data therefore support the hypothesis that synapses and axons play a key

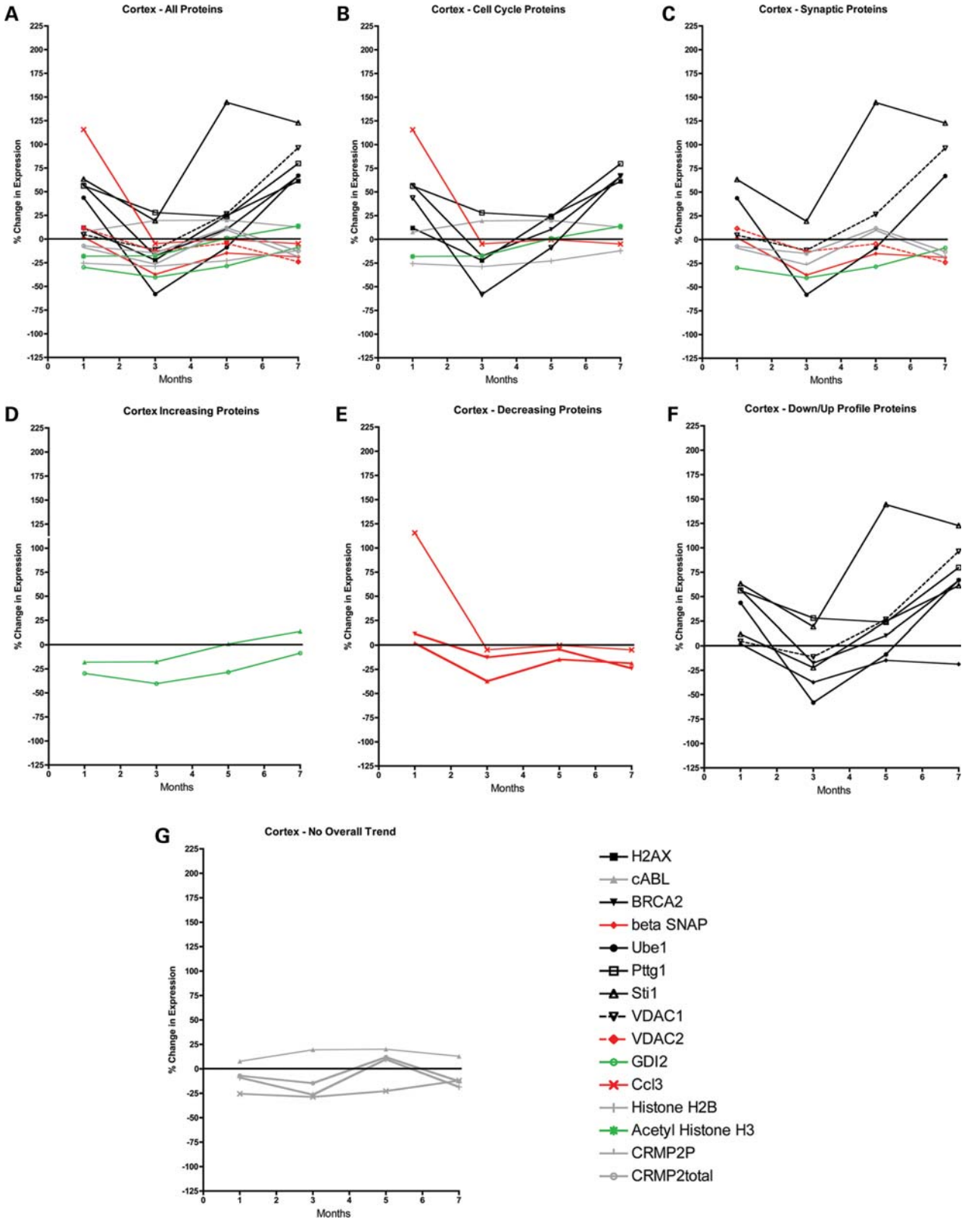

Figure 5. Temporal progression of protein expression changes in the cortex of *Ppt1*$^{-/-}$ mice. (**A**) Temporal progression of expression profiles for all 15 proteins examined. This graph is included to illustrate the overall complexity of expression changes observed. Data for individual proteins is shown more clearly on the subsequent graphs. (**B**) Graph of cell cycle proteins only [data extracted from (A)]. (**C**) Graph of synaptic proteins only [data extracted from (A)]. (**D**–**G**) Graphs showing expression levels for proteins conforming to a 'increasing' profile (D), 'decreasing' profile (E), 'down-up' profile (F) or 'no overall trend' profile (G). Profiles were determined by the patterns of change in expression following initial measurements in 1-month-old mice, not by the initial direction of change. Note how proteins conforming to the 'down-up' profile reach their peak in 3-month-old mice. All data normalized to control tubulin levels.

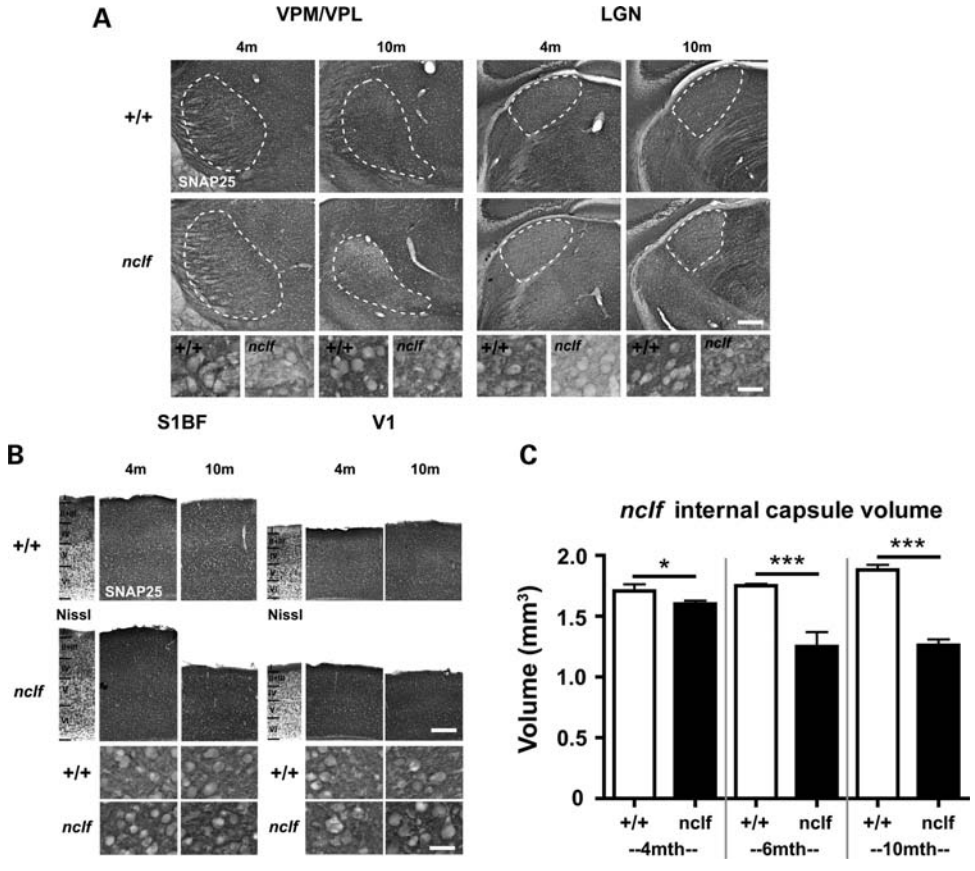

Figure 6. Synaptic and axonal pathology in early-symptomatic *Cln6*^{nclf} mice **(A)** Changes in the distribution and intensity of staining for SNAP25 in the ventral posteromedial and ventral posterolateral (VPM/VPL) and dorsal lateral geniculate (LGN) thalamic nuclei of 4 and 10-month-old *Cln6*^{nclf} deficient mice (*nclf*) and controls (+/+). SNAP25 immunoreactivity was markedly reduced in the thalamus of *Cln6*^{nclf} mice at 4 months of age and was decreased further at 10 months of age in *Cln6*^{nclf} mice, as revealed in more detail at higher magnification. The boundaries of thalamic nuclei are indicated by white dashed lines. **(B)** SNAP25 immunoreactivity was already elevated compared with controls (+/+) at 4 months of age, and was subsequently more intense in *Cln6*^{nclf} mice at 10 months of age. Laminar boundaries are indicated by roman numerals on a Nissl-stained section through the same region of cortex. **(C)** Stereological survey of internal capsule volume in control and *Cln6*^{nclf} tissue at different stages of disease progression. The volume of the internal capsule was significantly reduced in *Cln6*^{nclf} mice versus controls from 4 months of age onwards. This reduction increased with time to reach a 40% difference between *Cln6*^{nclf} mice and age-matched controls at 10 months of age. (mean ± SEM; $^{**}P < 0.01$; $^{***}P < 0.001$; ANOVA with *post-hoc* Bonferroni analysis). (**A** and **B**) show representative images from experiments on >3 mice per genotype. Scale bar = 200 μm in (**A** and **B**); 30 μm in higher magnification views.

role in the onset and progression of neurodegeneration in the NCLs, supporting the findings of several other recent studies (16–18). As such, the NCLs may need to be considered, along with many other diseases of the CNS and PNS (including Alzheimer's disease and motor neuron diseases such as amyotrophic lateral sclerosis and spinal muscular atrophy) (34–36), as 'synaptopathies' and/or 'distal axonopathies' (reviewed in 37). Treatments that can directly target axonal and synaptic compartments of neurons may therefore slow or halt the onset and/or progression of NCL neuropathology.

Our finding that several proteins whose expression profiles are known to reflect the vulnerability status of axons and synapses have modified expression levels in the brains of two NCL mouse models provides further evidence in support of synaptic and axonal vulnerability in these disorders. The data showing that several of these synaptic proteins have modified expression levels pre/early-symptomatically in NCL mice suggests that synaptic changes at the molecular level are instigated in advance of any overt neuropathological changes. Interestingly, several of the early expression changes observed in NCL mouse models (e.g. VDAC1) occurred in the opposite direction to those found in *Wld*^{s}-expressing cells. However, it is difficult to directly compare expression changes of individual proteins in NCL mouse models with those found in *Wld*^{s}-expressing cells. This is due to the fact that the *Wld*^{s} phenotype remains constant (in the tissues used to measure protein expression) while disease progression in NCL is very dynamic, with corresponding fluxes in expression levels (Figs 3 and 5). It would, however, be of interest to establish whether crossing *Wld*^{s} mice with mouse models of NCL has any therapeutic benefit. Such crosses would also be useful for further investigations into the roles of individual proteins identified in the current study.

Interestingly, several of the protein changes we have identified in the current study correspond to data presented in reports on previous microarray experiments carried out on either whole brain or cortical tissue from mouse models of Batten disease (38,39). These changes included Pttg1, histone H2B, CCL3. The modest magnitude of changes in these genes (and those in other corresponding pathways) is

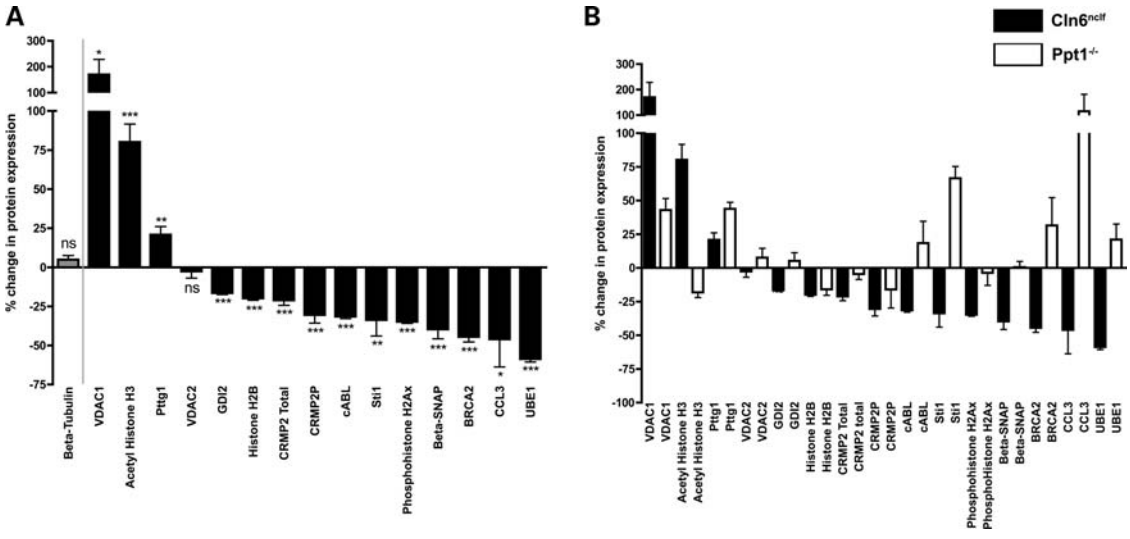

Figure 7. Protein expression changes in the thalamus of early-symptomatic (3 month old) *Cln6*^{nclf} mice compared with early-symptomatic (1 month old) *Ppt1*$^{-/-}$ mice reveal VDAC1 and Pttg1 as potential biomarkers of axonal and synaptic vulnerability. (**A**) Bar chart showing percentage changes in expression levels for all 15 proteins examined in *Cln6*^{nclf} mice (as well as tubulin control levels), compared with wild-type littermate controls. Statistical values were calculated using unpaired *t*-tests on raw arbitrary fluorescence values from *Cln6*^{nclf} mice compared with wild-type littermate controls. Note that all but one of the experimental proteins (VDAC2) had significant changes in expression levels in the *Cln6*^{nclf} mice. (**B**) Bar chart showing expression levels (normalized to tubulin) for all 15 proteins examined. Black bars show data from *Cln6*^{nclf} mice and white bars show data from *Ppt1*$^{-/-}$ mice (mean $\pm$ SEM; $n = 3$ mice per genotype/protein). Note the distinct expression profiles between the two groups of mice: only 5 out of the 15 proteins examined showed expression changes consistently changing in the same direction. Two of the proteins examined, however, showed robust increases in expression levels in both mouse models (VDAC1 and Pttg1). Expression data for CRMP2 total and CRMP2P in *Cln6*^{nclf} mice are the same as those previously published in (62).

likely to reflect the heterogeneous nature of the tissue samples used for the microarray experiments, which did not focus on the thalamus, the core location of early pathological changes in these forms of NCL. This suggests that repeating microarray experiments on isolated thalamic tissue might provide additional important insights into pathways and proteins beyond the scope of the current study.

The finding that several cell-cycle-related proteins have modified expression levels provides evidence that the cell-cycle status of terminally differentiated neurons and/or their supporting cells is altered in the NCLs. This finding is in keeping with a growing body of papers showing that altered cell-cycle status can contribute significantly to neurodegenerative disease. For example, numerous examples of cell-cycle regulation gone awry have been reported in neurodegenerative conditions such as motor neuron disease, Alzheimer's disease, Parkinson's disease and stroke (40,41,63,64). Furthermore, pharmacological manipulation of cell-cycle progression has been used to confer neuroprotection in animal models of traumatic brain injury and stroke (42,43). Our data support the hypothesis that the influence of cell-cycle status on neuronal vulnerability extends beyond neurodegenerative mechanisms resident in cell soma to incorporate independent degenerative pathways in axonal and synaptic compartments (31). Cell-cycle pathways may therefore constitute viable therapeutic targets for the treatment of NCL pathology.

One particularly novel finding of the current study was the distinct temporal profiles of protein expression occurring in the thalamus and cortex of *Ppt1*$^{-/-}$ mice. The finding that some proteins had increased expression levels with disease progression rules out the possibility that the protein changes observed were simply occurring due to a loss of total neuronal protein content. Moreover, the identification of 'up-down' profiles in the thalamus and 'down-up' profiles in the cortex, with peaks occurring in 3-month-old mice, suggests that the expression levels of several proteins were intimately associated with the instigation of synaptic and axonal pathology (as evidenced by our morphological studies; Fig. 1). We have previously shown that pathological events in *Ppt1*$^{-/-}$ mice are progressive, with acute astrocytosis first appearing at 3 months of age in specific thalamic nuclei, followed by loss of neurons relaying different sensory modalities (44). This thalamic neuron loss was followed by loss of corresponding cortical target granule neurons that were only significantly affected in the later stages of disease progression (44). The age of 3 months in *Ppt1*$^{-/-}$ mice therefore appears to be a major turning point in the pathogenesis of this disorder, as this is the point in disease expression when synapse loss (and associated protein expression changes), axon loss and astrocytosis are all triggered.

The finding that protein expression changes in the cortex did not precisely mirror those identified in the thalamus is perhaps not surprising given our understanding of the different progression of disease-associated pathology in these regions (44). Moreover, it has previously been suggested that synaptic reorganization or plasticity may occur in the cortex as a compensatory mechanism against ongoing neuron loss within the thalamus (17) (J Cooper and T Gillingwater, unpublished observations). Our morphological data showing more adaptive changes in synaptic protein levels in the cortex of *Ppt1*$^{-/-}$ mice supports this hypothesis.

Despite the obvious differences in expression profiles for proteins in the thalamus and cortex, one protein in *Ppt1*$^{-/-}$ mice (Ccl3) displayed a similar expression profile in both regions, with a very high expression at 1 month of age fol-

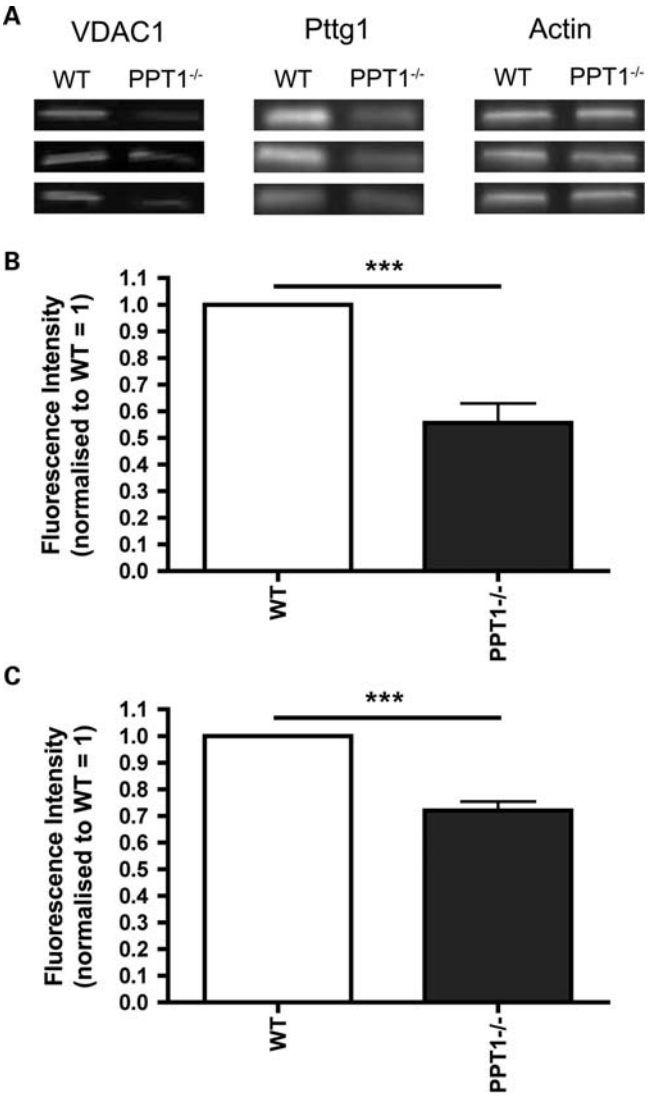

Figure 8. VDAC1 and Pttg1 protein expression changes were also detectable in peripherally accessible muscle tissue from 1-month-old $Ppt1^{-/-}$ mice. (**A**) Bands from quantitative fluorescent western blots showing significantly reduced expression levels of both VDAC1 and Pttg1 in 1-month-old $Ppt1^{-/-}$ mice (example blots from three separate animals are shown to illustrate variability between samples). Actin is shown as a loading control. (**B**) Bar chart showing a significant reduction in VDAC1 levels in muscle tissue from 1-month-old $Ppt1^{-/-}$ mice ($^{***}P < 0.001$, Mann–Whitney test, $n = 4$ mice per genotype). (**C**) Bar chart showing a significant reduction in Pttg1 levels in muscle tissue from 1-month-old $Ppt1^{-/-}$ mice ($^{***}P < 0.001$, Mann–Whitney test, $n = 4$ mice per genotype).

lowed by a dramatic decrease from 3 months onwards. This finding is of potential interest because Ccl3 protein, also known as macrophage inflammatory protein 1α (MIP-1α), is a chemokine involved in inflammation (45,46). CNS inflammation is evident in all forms of NCL (44,47–49), and also in other neurodegenerative disorders (50–52). For example, elevated levels of Ccl3/MIP-1α were found in a mouse model of Sandhoff disease *(*$Hexb^{-/-}$*)*, another lysosomal storage disorder, and loss of MIP-1α improves disease phenotype (53). Our finding therefore supports that hypothesis that inflammation may contribute to neurodegeneration in $Ppt1^{-/-}$ mice. However, a lack of similar initially increased expression levels of Ccl3 in $Cln6^{nclf}$ mice suggests that the inflammatory response is not necessarily conserved between different forms of the NCLs. It may therefore be informative to determine whether upregulation of Ccl3/MIP-1α occurs in other forms of NCL.

Perhaps the most exciting finding of the present study is that modified expression levels of two distinct proteins (VDAC1 and Pttg1) robustly occur during the pre/early-symptomatic stages of disease progression in both mouse models of NCL examined. The role of these proteins in axonal and synaptic pathology remains unclear, although previous studies have suggested that Pttg1 may modify ubiquitination pathways in synapses and axons (29,31) and VDAC1 is known to be a core regulator of mitochondrial form and function (30). However, our findings suggest that VDAC1 and Pttg1 proteins are likely to be useful biomarkers of early changes in axonal and synaptic vulnerability in INCL and vLINCL, reporting on molecular changes occurring in advance of morphological events. These proteins have potential advantages over previously proposed biomarkers—lysosomal acid phosphotase (54) and transcriptional changes in extracellular matrix proteins (55)—because they specifically report upon changes occurring in biologically relevant neuronal compartments (axons and synapses), can be detected in peripherally accessible muscle samples and appear to be conserved across multiple different forms of NCL. It will now be of particular importance to examine whether similar changes in these proteins occur across other animal models of the NCLs as well as in human patients. As the current study was restricted to a relatively small number of previously identified proteins, experiments increasing the numbers and diversity of proteins examined may lead to the identification of additional potential biomarkers for altered axonal and synaptic vulnerability in NCL.

MATERIALS AND METHODS

Mouse models

The *Ppt1*-deficient mice ($Ppt1^{-/-}$) used in this study were originally created through a targeted disruption strategy which eliminates the last exon in the coding sequence of *Ppt1* (56). These mice were subsequently backcrossed for 10 generations with C57BL/6 control mice, which is generally considered sufficient to be congenic on this strain background. C57BL/6 congenic $Ppt1^{-/-}$ mice and age-matched C57BL/6 control mice were bred and housed in a barrier facility at Washington University School of Medicine (St Louis, MO). C57BL/6 congenic $Cln6^{nclf}$ mice and C57BL/6 control mice were originally obtained from The Jackson Laboratory (Bar Harbour, ME) and were bred and housed in the vivarium at University of Rochester School of Medicine and Dentistry (Rochester, NY). All diseased and control mice used in this study were littermates. All animal procedures were carried out in accordance with NIH guidelines and the Institutional Animal Care and Use Committee regulations of Washington University and the University of Rochester.

Histological analysis

Ppt1$^{-/-}$ mice present with an INCL-related phenotype and usually die around 8–8.5 months of age (56). In contrast, *Cln6*^{nclf} mice model a vLINCL phenotype and live until 12 months of age (57). To analyse the progression of synaptic and axonal pathological changes in the *Ppt1*$^{-/-}$ deficient CNS, the brains of *Ppt1*$^{-/-}$ mice and C57BL/6 controls were harvested at 1, 3, 5 and 7 months of age ($n = 3$ *Ppt1*$^{-/-}$ and C57BL/6 control mice at each age). A similar analysis of the progression of synaptic and axonal pathological changes in the *Cln6* mice was performed on brains harvested at 4 and 10 months. Brains were immersion fixed for at least 1 week in 4% paraformaldehyde in 0.1 M phosphate-buffered saline, cryoprotected in a solution of 30% sucrose in Tris buffered saline (TBS: 50 mM Tris, pH 7.6, 150 mM NaCl) and 40 μm frozen coronal sections cut through the rostrocaudal extent of the cortical mantle (48,58,59). Sections were stored in a cryoprotectant solution (TBS/30% ethylene glycol/15% sucrose/0.05% sodium azide) at −40°C prior to histological processing.

Measurement of internal capsule volume

To provide direct visualization of the internal capsule (the white matter tract that connects the thalamus and cortex), every sixth section was slide mounted and Nissl stained as described previously (48). Unbiased Cavalieri estimates of the volume of the internal capsule were made from each animal with no prior knowledge of genotype. A sampling grid with appropriate spacing (150 μm) was superimposed over Nissl-stained sections and the number of points covering the relevant areas counted using ×2.5 objective. Regional volumes were expressed in mm^3 and the mean volume of each region calculated for control and *Ppt1*$^{-/-}$ or *nclf* mice. All volume analyses were carried out using *StereoInvestigator* software (Microbrightfield Inc., Williston, VT) on a Zeiss Axioskop2 MOT microscope (Carl Zeiss Ltd., Welwyn Garden City, UK) linked to a DAGE-MTI CCD-100 camera (DAGE-MTI Inc., Michigan City, IN, USA).

Immunohistochemical staining

To survey the expression of different synaptic markers, a one in six series of sections was immunohistochemically stained for presynaptic markers synaptophysin (Syp), synaptobrevin (VAMP2) and SNAP 25. These reactions used the following polyclonal primary antisera (monoclonal mouse anti-Syp, Upstate, 1 : 100; chicken anti-VAMP2, Chemicon, 1 : 500; monoclonal mouse anti-SNAP25, BD Transduction, 1 : 1000). Sections were then rinsed in TBS with subsequent incubation in secondary anti-serum (goat anti-mouse [Syp and SNAP25] and goat anti-chicken [VAMP2], Vector Laboratories, 1 : 1000) followed by avidin-biotin-peroxidase complex (Vectastain Elite ABC kit, Vector Laboratories). Immunoreactivity was visualized by a standard DAB reaction and sections were mounted onto slides, air-dried, cleared in xylene and coverslipped with DPX (VWR, Dorset, UK).

Protein expression analysis by quantitative immunofluorescence western blot

We used a quantitative immunofluorescence western blot approach because of its highly sensitive, reliable and reproducible nature (30,31,60). *Ppt1*$^{-/-}$ and *Cln6*^{nclf} brains, as well as brains from control littermates, were rapidly dissected immediately after sacrifice at different ages ($n = 3$ brains per genotype per time-point), bisected and flash frozen on dry ice. The left hemisphere of each brain was then dissected in order to produce separate samples containing thalamic (T) and cortical (C) tissue. Protein was extracted and assayed as previously described (30,31,60). Briefly, tissue was homogenized in 200 μl of ice-cold radioimmunoprecipitation (RIPA) buffer and 2 μl of protease inhibitors (Pierce Biosciences) before being gently passed through a 23G needle and a 25G needle to manually homogenize each sample. The homogenate was then centrifuged at 14 000 rpm for 20 min at 4°C. Finally, the supernatant was collected into a fresh tube and kept at −80°C until use. Protein concentration was determined through the use of a MicroBCA assay kit (Pierce Biosciences) as per manufacturer's instructions.

In order to separate the proteins according to their molecular weight, each sample was run on a 4–12% sodium dodecyl sulphate polyacrylamide pre-cast gel (SDS–PAGE) using a XCell *SureLock* Mini-Cell electrophoresis cell (Invitrogen). Fifteen micrograms of protein sample in a volume of 10 μl loading buffer (Pierce Biosciences) were prepared. Each sample was then boiled at 98°C for 2 min, spun down and loaded on the gel. The gel was subsequently run at 120 V for 45 min. The proteins were then transferred from the gel onto a PVDF membrane (Invitrogen). The transfer was run over night.

To visualize the changes in protein expression levels, PVDF membranes were probed using primary antibodies at 1 : 5000 dilution (Table 1) after incubation in Odyssey blocking buffer (Li-COR) for 45 min at room temperature. Membranes were rinsed 3 × 5 min with PBS-Tween 0.1% and incubated with appropriate fluorescent secondary antibodies secondary antibodies at 1 : 5000 dilution (Odyssey; Goat anti rabbit IRDye 680, Goat anti-mouse IRDye 800-Li-COR Biosciences; Donkey anti-sheep IRDye 800 -Rockland) for 1.5 h at room temperature in the dark. Beta-tubulin (Abcam) antibodies were used for loading controls wherever required. The validity of all antibodies used in current experiments has been confirmed in previous studies run in conjunction with proteomic and SuperArray screens (30,31). In addition, all antibodies used generated bands at the predicted molecular weight.

Immunoreactive bands were visualized using an Odyssey Infrared Imaging System (Li-COR Biosciences). Scan resolution of the instrument ranges from 21 to 339 μm and in this study blots were imaged at 169 μm. Quantification was performed on single channels with the analysis software provided. Blot scans were analysed using the Odyssey software to manually define bands. Odyssey software assigned arbitrary fluorescence values to these bands, to give relative fluorescence intensity between bands on each membrane. Three mice were used for each brain region and each was scanned three times at different laser intensities in order to minimize user error. This gave $n = 9$ scans, and $n = 3$ mice/membranes

per brain region for each protein (30,31). Representative blots were prepared for publication by exporting images from the Licor Odyssey software as TIFFs before converting to grey-scale images using Adobe Photoshop.

Muscle protein expression analysis

Hind-limb musculature from 1-month-old $Ppt1^{-/-}$ and wild-type littermate mice were rapidly dissected following sacrifice and flash frozen. Frozen muscle tissue was then homogenized using a pestle and mortar. Powdered muscle was solubilized, protein was extracted and samples processed as described earlier. Quantitative western blotting was performed as described earlier using antibodies against VDAC1, Pttg1 and actin (Abcam; used as a loading control).

Statistical analysis

The statistical significance of differences between genotypes of internal capsule volume measurements was assessed using a one-way ANOVA (SPSS 11.5 software, SPSS Inc., Chicago, IL), with statistical significance considered at $P \leq 0.05$. The mean co-efficient of error (CE) for all individual optical fractionator and Cavalieri estimates was calculated according to the method of Gundersen and Jensen (61) and was <0.08 in all these analyses. Data from the quantitative western blots was entered into Microsoft Excel and GraphPad Prism v.5 for further analysis. Statistical comparisons of protein expression levels between diseased mice and wild-type littermates were undertaken using an unpaired *t*-test, with statistical significance considered at $P \leq 0.05$ (ns = not significant; $^{*}P < 0.05$; $^{**}P < 0.01$; $^{***}P < 0.001$).

ACKNOWLEDGEMENTS

The authors would like to thank Derek Thomson and members of the Gillingwater, Parson and PSDL laboratories for helpful advice and assistance with this study and Dr Calum Sutherland (University of Dundee) for the gift of antibodies.

Conflict of Interest statement. None declared.

FUNDING

This work was supported by grants from the Wellcome Trust (grant WT084151AIA to T.H.G.; grant GR079491MA to J.D.C.); Biotechnology and Biological Sciences Research Council (grant BB/D001722/1 to T.H.G.); National Institutes of Health (grant NS41930 to J.D.C.; NS40580 and NS44310 to D.A.P.; NS043105 to M.S.S.); European Commission 6th Framework (grant LSHM-CT-2003-503051 to J.D.C.); Batten Disease Support and Research Association (to T.H.G./J.D.C./C.K. and D.A.P.); Natalie Fund (to J.D.C.); Batten Disease Family Association (to J.D.C./C.K.); and Remy Fund (to J.D.C.). Funding to pay the Open Access publication charges for this article was provided by the Wellcome Trust.

REFERENCES

1. Goebel, H.H. (1995) The neuronal ceroid-lipofuscinoses. *J. Child. Neurol.*, **10**, 424–437.
2. Cooper, J.D. (2003) Progress towards understanding the neurobiology of Batten disease or neuronal ceroid lipofuscinosis. *Curr. Opin. Neurol.*, **16**, 121–128.
3. Mole, S.E., Williams, R.E. and Goebel, H.H. (2005) Correlations between genotype, ultrastructural morphology and clinical phenotype in the neuronal ceroid lipofuscinoses. *Neurogenetics*, **6**, 107–126.
4. Santavuori, P. (1998) Neuronal ceroid-lipofuscinoses in childhood. *Brain Dev.*, **10**, 80–83.
5. Vesa, J., Hellsten, E., Verkruyse, L.A., Camp, L.A., Rapola, J., Santavuori, P., Hofmann, S.L. and Peltonen, L. (1995) Mutations in the palmitoyl protein thioesterase gene causing infantile neuronal ceroid lipofuscinosis. *Nature*, **376**, 584–587.
6. Hofmann, S.L., Atashband, A., Cho, S.K., Das, A.K., Gupta, P. and Lu, J.Y. (2002) Neuronal ceroid lipofuscinoses caused by defects in soluble lysosomal enzymes (CLN1 and CLN2). *Curr. Mol. Med.*, **2**, 423–437.
7. Haltia, M., Rapola, J. and Santavuori, P. (1973) Infantile type of so-called neuronal ceroid-lipofuscinosis. Histological and electron microscopic studies. *Acta Neuropathol.*, **26**, 157–170.
8. Haltia, M., Rapola, J., Santavuori, P. and Keränen, A. (1973) Infantile type of so-called neuronal ceroid-lipofuscinosis. 2. Morphological and biochemical studies. *J. Neurol. Sci.*, **18**, 269–285.
9. Santavuori, P., Lauronen, L., Kirveskari, K., Aberg, L. and Sainio, K. (2000) Neuronal ceroid lipofuscinoses in childhood. *Suppl. Clin. Neurophysiol.*, **53**, 443–451.
10. Gao, H., Boustany, R.M., Espinola, J.A., Cotman, S.L., Srinidhi, L., Antonellis, K.A., Gillis, T., Qin, X., Liu, S., Donahue, L.R. *et al.* (2002) Mutations in a novel CLN6-encoded transmembrane protein cause variant neuronal ceroid lipofuscinosis in man and mouse. *Am. J. Hum. Genet.*, **70**, 324–335.
11. Wheeler, R.B., Sharp, J.D., Schultz, R.A., Joslin, J.M., Williams, R.E. and Mole, S.E. (2002) The gene mutated in variant late-infantile neuronal ceroid lipofuscinosis (CLN6) and in nclf mutant mice encodes a novel predicted transmembrane protein. *Am. J. Hum. Genet.*, **70**, 537–542.
12. Heine, C., Koch, B., Storch, S., Kohlschütter, A., Palmer, D.N. and Braulke, T. (2004) Defective endoplasmic reticulum-resident membrane protein CLN6 affects lysosomal degradation of endocytosed arylsulfatase A. *J. Biol. Chem.*, **79**, 22347–22352.
13. Mole, S.E., Michaux, G., Codlin, S., Wheeler, R.B., Sharp, J.D. and Cutler, D.F. (2004) CLN6, which is associated with a lysosomal storage disease, is an endoplasmic reticulum protein. *Exp. Cell. Res.*, **298**, 399–406.
14. Lehtovirta, M., Kyttälä, A., Eskelinen, E.L., Hess, M., Heinonen, O. and Jalanko, A. (2001) Palmitoyl protein thioesterase (PPT) localizes into synaptosomes and synaptic vesicles in neurons: implications for infantile neuronal ceroid lipofuscinosis (INCL). *Hum. Mol. Genet.*, **10**, 69–75.
15. Luiro, K., Kopra, O., Lehtovirta, M. and Jalanko, A. (2001) CLN3 protein is targeted to neuronal synapses but excluded from synaptic vesicles: new clues to Batten disease. *Hum. Mol. Genet.*, **10**, 2123–2131.
16. Virmani, T., Gupta, P., Liu, X., Kavalali, E.T. and Hofmann, S.L. (2005) Progressively reduced synaptic vesicle pool size in cultured neurons derived from neuronal ceroid lipofuscinosis-1 knockout mice. *Neurobiol. Dis.*, **20**, 314–323.
17. Partanen, S., Haapanen, A., Kielar, C., Pontikis, C., Alexander, N., Inkinen, T., Saftig, P., Gillingwater, T.H., Cooper, J.D. and Tyynelä, J. (2008) Synaptic changes in the thalamocortical system of cathepsin D-deficient mice: a model of human congenital neuronal ceroid-lipofuscinosis. *J. Neuropathol. Exp. Neurol.*, **67**, 16–29.
18. Kim, S.J., Zhang, Z., Sarkar, C., Tsai, P.C., Lee, Y.C., Dye, L. and Mukherjee, A.B. (2008) Palmitoyl protein thioesterase-1 deficiency impairs synaptic vesicle recycling at nerve terminals, contributing to neuropathology in humans and mice. *J. Clin. Invest.*, **118**, 3075–3086.
19. Lunn, E.R., Perry, V.H., Brown, M.C., Rosen, H. and Gordon, S. (1989) Absence of Wallerian degeneration does not hinder regeneration in peripheral nerve. *Eur. J. Neurosci.*, **1**, 27–33.
20. Ludwin, S.K. and Bisby, M.A. (1992) Delayed Wallerian degeneration in the central nervous system of Ola mice: An ultrastructural study. *J. Neurol. Sci.*, **109**, 140–147.
21. Gillingwater, T.H., Thomson, D., Mack, T.G., Soffin, E.M., Mattison, R.J., Coleman, M.P. and Ribchester, R.R. (2002) Age-dependent synapse

withdrawal at axotomised neuromuscular junctions in Wld(s) mutant and Ube4b/Nmnat transgenic mice. *J. Physiol.*, **543**, 739–755.
22. Gillingwater, T.H., Ingham, C.A., Parry, K.E., Wright, A.K., Haley, J.E., Wishart, T.M., Arbuthnott, G.W. and Ribchester, R.R. (2006) Delayed synaptic degeneration in the CNS of Wlds mice after cortical lesion. *Brain*, **129**, 1546–1556.
23. Samsam, M., Mi, W., Wessig, C., Zielasek, J., Toyka, K.V., Coleman, M.P. and Martini, R. (2003) The Wlds mutation delays robust loss of motor and sensory axons in a genetic model for myelin-related axonopathy. *J. Neurosci.*, **23**, 2833–2839.
24. Ferri, A., Sanes, J.R., Coleman, M.P., Cunningham, J.M. and Kato, A.C. (2003) Inhibiting axon Inhibiting axon degeneration and synapse loss attenuates apoptosis and disease progression in a mouse model of motoneuron disease. *Curr Biol.*, **13**, 669–673.
25. Sajadi, A., Schneider, B.L. and Aebischer, P. (2004) Wlds-mediated protection of dopaminergic fibers in an animal model of Parkinson disease. *Curr. Biol.*, **14**, 326–330.
26. Gillingwater, T.H., Haley, J.E., Ribchester, R.R. and Horsburgh, K. (2004) Neuroprotection after transient global cerebral ischemia in Wld(s) mutant mice. *J. Cereb. Blood Flow Metab.*, **24**, 62–66.
27. Adalbert, R., Gillingwater, T.H., Haley, J.E., Bridge, K., Beirowski, B., Berek, L., Wagner, D., Grumme, D., Thomson, D., Celik, A. *et al.* (2005) A rat model of slow Wallerian degeneration (Wlds) with improved preservation of neuromuscular synapses. *Eur. J. Neurosci.*, **21**, 271–277.
28. MacDonald, J.M., Beach, M.G., Porpiglia, E., Sheehan, A.E., Watts, R.J. and Freeman, M.R. (2006) The Drosophila cell corpse engulfment receptor Draper mediates glial clearance of severed axons. *Neuron*, **50**, 869–881.
29. Gillingwater, T.H., Wishart, T.M., Chen, P.E., Haley, J.E., Robertson, K., MacDonald, S.H., Middleton, S., Wawrowski, K., Shipston, M.J., Melmed, S. *et al.* (2006) The neuroprotective WldS gene regulates expression of PTTG1 and erythroid differentiation regulator 1-like gene in mice and human cells. *Hum. Mol. Genet.*, **15**, 625–635.
30. Wishart, T.M., Paterson, J.M., Short, D.M., Meredith, S., Robertson, K.A., Sutherland, C., Cousin, M.A., Dutia, M.B. and Gillingwater, T.H. (2007) Differential proteomics analysis of synaptic proteins identifies potential cellular targets and protein mediators of synaptic neuroprotection conferred by the slow Wallerian degeneration (Wlds) gene. *Mol. Cell. Proteomics.*, **6**, 1318–1330.
31. Wishart, T.M., Pemberton, H.N., James, S.R., McCabe, C.J. and Gillingwater, T.H. (2008) Modified cell cycle status in a mouse model of altered neuronal vulnerability (slow Wallerian degeneration; Wlds). *Genome Biol.*, **9**, R101.
32. Shi, M.M., Godleski, J.J. and Paulauskis, J.D. (1996) Regulation of macrophage inflammatory protein-1alpha mRNA by oxidative stress. *J. Biol. Chem.*, **271**, 5878–5883.
33. Lässle, M., Blatch, G.L., Kundra, V., Takatori, T. and Zetter, B.R. (1997) Stress-inducible, murine protein mSTI1. Characterization of binding domains for heat shock proteins and in vitro phosphorylation by different kinases. *J. Biol. Chem.*, **272**, 1876–1884.
34. Selkoe, D.J. (2002) Alzheimer's disease is a synaptic failure. *Science*, **298**, 789–791.
35. Fischer, L.R., Culver, D.G., Tennant, P., Davis, A.A., Wang, M., Castellano-Sanchez, A., Khan, J., Polak, M.A. and Glass, J.D. (2004) Amyotrophic lateral sclerosis is a distal axonopathy: evidence in mice and man. *Exp. Neurol.*, **185**, 232–240.
36. Murray, L.M., Comley, L.H., Thomson, D., Parkinson, N., Talbot, K. and Gillingwater, T.H. (2008) Selective vulnerability of motor neurons and dissociation of pre- and post-synaptic pathology at the neuromuscular junction in mouse models of spinal muscular atrophy. *Hum. Mol. Genet.*, **17**, 949–962.
37. Wishart, T.M., Parson, S.H. and Gillingwater, T.H. (2006) Synaptic vulnerability in neurodegenerative disease. *J. Neuropathol. Exp. Neurol.*, **65**, 733–739.
38. Qiao, X., Lu, J.Y. and Hofmann, S.L. (2007) Gene expression profiling in a mouse model of infantile neuronal ceroid lipofuscinosis reveals upregulation of immediate early genes and mediators of the inflammatory response. *BMC Neurosci.*, **8**, 95.
39. von Schantz, C., Saharinen, J., Kopra, O., Cooper, J.D., Gentile, M., Hovatta, I., Peltonen, L. and Jalanko, A. (2008) Brain gene expression profiles of Cln1 and Cln5 deficient mice unravels common molecular pathways underlying neuronal degeneration in NCL diseases. *BMC Genomics*, **9**, 146.
40. Höglinger, G.U., Breunig, J.J., Depboylu, C., Rouaux, C., Michel, P.P., Alvarez-Fischer, D., Boutillier, A.L., Degregori, J., Oertel, W.H., Rakic, P. *et al.* (2007) The pRb/E2F cell-cycle pathway mediates cell death in Parkinson's disease. *Proc. Natl Acad. Sci. USA*, **104**, 3585–3590.
41. Love, S. (2003) Neuronal expression of cell cycle-related proteins after brain ischaemia in man. *Neurosci. Lett.*, **353**, 29–32.
42. Di Giovanni, S., Movsesyan, V., Ahmed, F., Cernak, I., Schinelli, S., Stoica, B. and Faden, A.I. (2005) Cell cycle inhibition provides neuroprotection and reduces glial proliferation and scar formation after traumatic brain injury. *Proc. Natl Acad. Sci. USA*, **102**, 8333–8338.
43. Wang, F., Corbett, D., Osuga, H., Osuga, S., Ikeda, J.E., Slack, R.S., Hogan, M.J., Hakim, A.M. and Park, D.S. (2002) Inhibition of cyclin-dependent kinases improves CA1 neuronal survival and behavioral performance after global ischemia in the rat. *J. Cereb. Blood Flow Metab.*, **22**, 171–182.
44. Kielar, C., Maddox, L., Bible, E., Pontikis, C.C., Macauley, S.L., Griffey, M.A., Wong, M., Sands, M.S. and Cooper, J.D. (2007) Successive neuron loss in the thalamus and cortex in a mouse model of infantile neuronal ceroid lipofuscinosis. *Neurobiol. Dis.*, **25**, 150–162.
45. Cook, D.N., Beck, M.A., Coffman, T.M., Kirby, S.L., Sheridan, J.F., Pragnell, I.B. and Smithies, O. (1995) Requirement of MIP-1 alpha for an inflammatory response to viral infection. *Science*, **269**, 1583–1585.
46. Krathwohl, M.D. and Kaiser, J.L. (2004) Chemokines promote quiescence and survival of human neural progenitor cells. *Stem Cells*, **22**, 109–118.
47. Pontikis, C.C., Cella, C.V., Parihar, N., Lim, M.J., Chakrabarti, S., Mitchison, H.M., Mobley, W.C., Rezaie, P., Pearce, D.A. and Cooper, J.D. (2004) Late onset neurodegeneration in the Cln3−/− mouse model of juvenile neuronal ceroid lipofuscinosis is preceded by low level glial activation. *Brain Res.*, **1023**, 231–242.
48. Bible, E., Gupta, P., Hofmann, S.L. and Cooper, J.D. (2004) Regional and cellular neuropathology in the palmitoyl protein thioesterase-1 null mutant mouse model of infantile neuronal ceroid lipofuscinosis. *Neurobiol. Dis.*, **16**, 346–359.
49. Kay, G.W., Palmer, D.N., Rezaie, P. and Cooper, J.D. (2006) Activation of non-neuronal cells within the prenatal developing brain of sheep with neuronal ceroid lipofuscinosis. *Brain Pathol.*, **16**, 110–116.
50. Danton, G.H. and Dietrich, W.D. (2003) Inflammatory mechanisms after ischemia and stroke. *J. Neuropathol. Exp. Neurol.*, **62**, 127–136.
51. Carson, M.J. (2002) Microglia as liaisons between the immune and central nervous systems: functional implications for multiple sclerosis. *Glia*, **40**, 218–231.
52. Eikelenboom, P., Bate, C., Van Gool, W.A., Hoozemans, J.J., Rozemuller, J.M., Veerhuis, R. and Williams, A. (2002) Neuroinflammation in Alzheimer's disease and prion disease. *Glia*, **40**, 232–239.
53. Wu, Y.P. and Proia, R.L. (2004) Deletion of macrophage-inflammatory protein 1 alpha retards neurodegeneration in Sandhoff disease mice. *Proc. Natl Acad. Sci. USA*, **101**, 8425–8430.
54. Pohl, S., Mitchison, H.M., Kohlschütter, A., Van Diggelen, O., Braulke, T. and Storch, S. (2007) Increased expression of lysosomal acid phosphatase in CLN3-defective cells and mouse brain tissue. *J. Neurochem.*, **103**, 2177–2188.
55. Teixeira, C.A., Lin, S., Mangas, M., Quinta, R., Bessa, C.J., Ferreira, C., Sá Miranda, M.C., Boustany, R.M. and Ribeiro, M.G. (2006) Gene expression profiling in vLINCL CLN6-deficient fibroblasts: Insights into pathobiology. *Biochim. Biophys. Acta.*, **1762**, 637–646.
56. Gupta, P., Soyombo, A.A., Atashband, A., Wisniewski, K.E., Shelton, J.M., Richardson, J.A., Hammer, R.E. and Hofmann, S.L. (2001) Disruption of PPT1 or PPT2 causes neuronal ceroid lipofuscinosis in knockout mice. *Proc. Natl Acad. Sci. USA*, **98**, 13566–13571.
57. Bronson, R.T., Donahue, L.R., Johnson, K.R., Tanner, A., Lane, P.W. and Faust, J.R. (1998) Neuronal ceroid lipofuscinosis (nclf), a new disorder of the mouse linked to chromosome 9. *Am. J. Med. Genet.*, **77**, 289–297.
58. Griffey, M., Bible, E., Vogler, C., Levy, B., Gupta, P., Cooper, J. and Sands, M.S. (2004) Adeno-associated virus 2-mediated gene therapy decreases autofluorescent storage material and increases brain mass in a murine model of infantile neuronal ceroid lipofuscinosis. *Neurobiol. Dis.*, **16**, 360–369.
59. Griffey, M., Macauley, S.L., Ogilvie, J.M. and Sands, M.S. (2005) AAV2-mediated ocular gene therapy for infantile neuronal ceroid lipofuscinosis. *Mol. Ther.*, **12**, 413–421.
60. Murray, L.M., Thomson, D., Conklin, A., Wishart, T.M. and Gillingwater, T.H. (2008) Loss of translation elongation factor (*eEF1A2*) expression

in vivo differentiates between Wallerian degeneration and dying-back neuronal pathology. *J. Anat.*, **213**, 633–645.
61. Gundersen, H.J. and Jensen, E.B. (1987) The efficiency of systematic sampling in stereology and its prediction. *J. Microsc.*, **147**, 229–263.
62. Benedict, J.W., Getty, A.L., Wishart, T.M., Gillingwater, T.H. and Pearce, D.A. (2009) The protein product of the CLN6 gene responsible for variant late-onset infantile neuronal ceroid lipofuscinosis interacts with CRMP-2. *J. Neurosci. Res.*, **87**, 2157–2166.
63. Ranganathan, S. and Bowser, R. (2003) Alterations in G(1) to S phase cell-cycle regulators during amyotrophic lateral sclerosis. *Am. J. Pathol.*, **162**, 823–835.
64. Vincent, I., Rosado, M. and Davies, P. (1996) Mitotic mechanisms in Alzheimer's disease? *J. Cell. Biol.*, **132**, 413–425.